ACS OMEGA

Open Access

http://pubs.acs.org/journal/acsodf

Article

Mechanosynthesis of Stable Salt Hydrates of Allopurinol with Enhanced Dissolution, Diffusion, and Pharmacokinetics

Richu Bagya Varsa S, Noopur Pandey, Animesh Ghosh, Anubha Srivastava, Pavan Kumar Puram, Sai Teja Meka, Vladimir V. Chernyshev,* and Palash Sanphui*

Cite This: *ACS Omega* 2023, 8, 34120−34133

Read Online

ACCESS | Metrics & More | Article Recommendations | Supporting Information

ABSTRACT: Allopurinol (ALO) is a medication that treats gout and kidney stones by lowering uric acid synthesis in the blood. The biopharmaceutics classification system (BCS) IV drug exhibits poor aqueous solubility, permeability, and bioavailability. To overcome the bottlenecks of ALO, salts with maleic acid (MLE) and oxalic acid (OXA) were synthesized using the solvent-assisted grinding method. The novel multicomponent solids were characterized by PXRD, DSC, TGA, FT-IR, and SEM images. The crystal structures of these salts with variable stoichiometry were obtained using Rietveld refinement from the high-resolution PXRD data. The proton from the dicarboxylic acid is transferred to the most basic pyrimidine "N" of ALO. The N−H···N hydrogen-bonded ALO homodimer is replaced by the N^+−H···O^- ionic interactions in ALO−OXA (2:1:0.4) and ALO−MLE (1:1:1) salt hydrates. The organic salts improved solubility and dissolution up to 5-fold and the diffusion permeability up to 12 times compared to the native drug in a luminal pH 6.8 phosphate buffer medium. The salt hydrates were exceptionally stable during storage at 30 ± 5 °C and 75 ± 5% relative humidity. Superior dissolution and diffusion permeability of the ALO−MLE salt resulted in improved pharmacokinetics (peak plasma concentration) that offers a promising solid dosage form with enhanced bioavailability and lower dosage formulation.

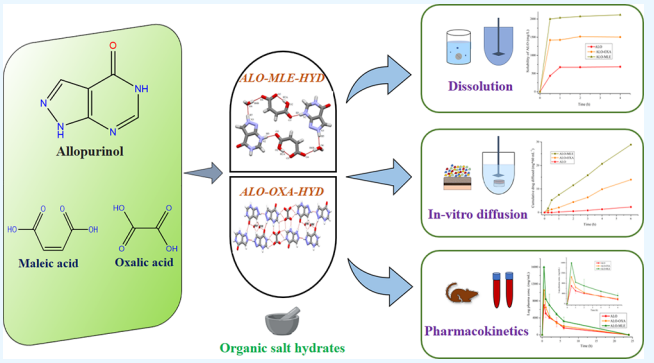

1. INTRODUCTION

Oral administration of active pharmaceutical ingredients (APIs) is the most preferred route of drug delivery due to ease of administration, affordable costs, and extended shelf life.[1] The major bottleneck of an oral formulation is that a drug should have sufficient solubility, permeability, and chemical stability to overcome the adverse effect of biological pH (1−6.8) during its journey through the gastrointestinal tract. Reduced solubility/permeability often decreases the shelf life/bioavailability of a drug, which indirectly obliges a formulation chemist to increase the dose limit for its suitable clinical activities. More than 10% of the marketed drug formulations are in the category of BCS class IV with shortcomings of aqueous solubility and permeability that result in poor bioavailability. Crystal engineering plays an important role in modulating the drug properties using multicomponent solid forms (e.g., cocrystals, salts, and eutectics).[2] In addition, decreasing particle size (e.g., nanocrystals), micelle formation, use of water-soluble additives/excipients (e.g., sodium lauryl sulfate and cellulose), hydrotropes, amorphous solid dispersion, etc. often increase the solubility/bioavailability of a drug.[3] These technologies have both merits and demerits. Comparatively, salts are the most acceptable multicomponent solid forms to improve dissolution and pharmacokinetics. In this scenario, solid-form screening is an essential component during the pre-formulation phase of a drug development following the filing of an innovator (synthesis/prior art) patent.[4] Solubility (related to hydrophilicity) and permeability (dependent on lipophilicity) are supposed to be the opposing factors. However, recent literature suggests that using cocrystals/salts, one can improve permeability through the intestinal membrane by increasing the solubility of a drug.[5−7] Similar to solubility factors, the reason (e.g., hydrophobic interactions/stacking interactions, concentration gradient, loose packing, and log *P* of the coformer) behind an improved permeability needs to be thoroughly understood.[8] Intense research on the preparation of multicomponent solid forms to improve the physicochemical properties of drugs yields novel marketed formulations with enhanced clinical efficacy.

Pharmaceutical salts as ionic hydrogen-bonded complexes are highly recommended to improve dissolution, absorption,

Received: July 22, 2023
Accepted: August 31, 2023
Published: September 7, 2023

and onset of the biological action of a drug.[9] In fact, more than 50% marketed drugs are available in the form of salts. Salt formation requires one ionizable API and a coformer/biologically safe molecule. A more significant ΔpK_a variation between an API and a coformer (usually ΔpK_a >4.0) can lead to the formation of salts.[10] Salts generally improve the solubility of a drug up to 10−100-fold and permeability up to 10-fold than its native free acid/base.[11,12] The major bottleneck of a salt is its hygroscopic nature that often compels a formulation chemist to design coated tablets to avoid moisture absorption. Hydrochloride and sodium salts are the top most preferred solid forms in the commercialized formulations of poor aqueous soluble drugs.[9] In addition, organic molecular salts are also becoming popular and commercialized (e.g., escitalopram oxalate, chlorpheniramine maleate, trelagliptin succinate, etc.). Bioavailability of a drug depends upon both solubility and permeability.[13] To enhance the permeability of a basic drug, coformers with higher log *P* values like cinnamic acid (log *P* = 2.14), salicylic acid (log *P* = 2.26), and 2,6-dihydroxybenzoic acid (log *P* = 2.14) may be recommended.[7,14] Highly soluble coformers like malonic acid (763 g/L), maleic acid (788 g/L), and glutaric acid (1600 g/L) can be employed to enhance the solubility of a low-soluble basic drug.[15−17] The selection of a suitable counterion determines the solid-state properties of a particular drug.

Allopurinol (hereafter ALO, chemical name: 1*H*-pyrazolo-[3,4-*d*]pyrimidine-4(2*H*)-one) is generally prescribed to treat high blood uric acid levels by inhibiting the enzyme xanthine oxidase.[18] It treats hyperuricemia, gout, uric acid, and kidney stones. It is considered as the World Health Organization's list of essential medicines and 42nd most commonly prescribed medication in the United States. The drug exhibits a high melting point (390 °C) that may be one of the reasons behind its poor aqueous solubility (800 mg/L) and permeability (log *P* = −1.8).[19] Due to its poor physicochemical properties, the drug is quickly metabolized within 2 h of oral administration. ALO is reported to crystalize as monomorph, hydrochloride, sulfate salts, and cocrystals with piperazine, pyridine 2,4-dicarboxylic acid, 2,4-dihydroxybenzoic acid, and isonicotinamide.[20−24] Recently, Dai et al. reported the improved diffusion properties of ALO up to 40% using cocrystals with 2,4-dihydroxybenzoic acid and piperazine.[24] In addition, attempts were made to enhance the solubility of ALO using prodrug formulations, solid dispersions, etc.[25,26] One can transform a BCS class IV drug, e.g., ALO, into a class I drug of high solubility/permeability using a crystal engineering tool. To enhance the solubility/permeability of ALO, organic molecular salts with oxalic acid and maleic acid in variable stoichiometry were synthesized using liquid-assisted grinding. Figure 1 represents ALO and its successful salt coformers wherein the most basic nitrogen (tertiary amine) of pyrimidine is marked

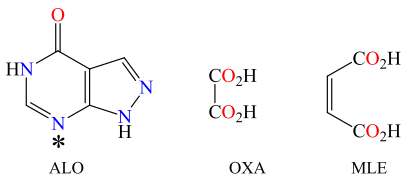

Figure 1. Chemical diagram of ALO and the dicarboxylic acid coformers used for the salt synthesis. ALO with the most basic "N" atom is represented as an asterisk that is easy to protonate in the presence of strong mineral acids.

to get protonated. The salts were characterized by PXRD, DSC, TGA, FT-IR, and SEM images.[27] In addition, their crystal structures were obtained by high-resolution XRD data as the salts exhibited high tendency to dissociate in the aqueous medium during cocrystallization. Finally, the ALO salts improved the dissolution, diffusion, and pharmacokinetics of ALO in a pH 6.8 phosphate buffer medium.

2. MATERIALS AND METHODS

2.1. Materials. ALO (purity 99.8%) was obtained as a gift sample from Lupin Ltd., Mumbai. The drug was also extracted from the commercialized Zyloprim (300 mg) tablets. Extraction was carried out by grinding and dissolving the tablets in a minimum amount of *N*,*N*-dimethylformamide and then adding the solution dropwise into a 10-fold volume of ice-cold distilled water. The anti-solvent crystallization resulted in an immediate white precipitate that was filtered and dried in a vacuum oven. PXRD data of the residual white mass was recorded and compared with the reported crystal structure of ALO (CCDC refcode: ALOPUR). The overlay of XRD comparison confirmed the purity of the drug (refer Figure S1, Supporting Information (SI)).

The carboxylic acid coformers oxalic acid, malonic acid, maleic acid, fumaric acid, succinic acid, glutaric acid, adipic acid, malic acid, tartaric acid, citric acid, ferulic acid, and vanillic acid, amides (nicotinamide and urea), and amino acids (L-arginine, L-lysine, and L-histidine) were procured from Sigma-Aldrich, Bangalore, and used as it is. Solvents (e.g., *N*,*N*-dimethylformamide, ethanol, and methanol) were obtained from SRL, Chennai.

2.2. Synthesis of ALO Salts. ALO and di-/tricarboxylic acids (1:1) were ground using a mortar and pestle with the addition of either MeOH−water (1:1) or EtOH−water (2:1) medium. Except ALO−MLE and ALO−OXA, most often, mechanosynthesis resulted in a physical mixture only. The partially wet ground material was dried under vacuum and checked with PXRD.

2.2.1. ALO−MLE. One equivalent each of ALO (136.1 mg, 1 mmol) and MLE (116.1 mg, 1 mmol) was ground in a mortar and pestle with the dropwise addition of EtOH:water (2:1) as a mixture of solvent for 15−20 min. The melting point of the ground mixture was 153−155 °C.

2.2.2. ALO−OXA. Two equivalents of ALO (272.2 mg, 2 mmol) was ground with 1.1 equiv of oxalic acid dihydrate (138.7 mg, 1.1 mmol) using MeOH:water (1:1) as a solvent for 15−20 min. The melting point of the ground mixture was 239−241 °C. Note that grinding of ALO:OXA (1:1) resulted a new XRD pattern with additional minor diffraction peaks of oxalic acid dihydrate.

The purity of the ALO and its salts were confirmed from their ^{1}H NMR spectra using DMSO-d_6 as a solvent (refer Figure S2, SI). The chemical shift values were provided below in terms of ppm.

ALO: (^{1}H NMR, 500 MHz, δ ppm) 8.00 (aromatic CH, 2H, s), 12.02 (NH, 1H, s), 13.75 (NH, 1H, s); ALO−MLE: 6.26 (aliphatic CH, 2H, s), 8.01 (aromatic CH, 1H, s), 8.12 (aromatic CH, 1H, s), 8.32 (NH, 1H, s), 12.01 (NH, 1H, s); ALO−OXA: 8.00 (aromatic CH, 2H, s), 8.12 (NH, 1H, s), 11.99 (NH, 1H, s).

2.3. Powder X-ray Diffraction (PXRD). PXRD data of ALO, acidic coformers, and the corresponding ground mixtures were recorded in a PANalytical X'Pert Pro X-ray powder diffractometer (Malvern PANalytical X'Pert 3, Nether-

https://doi.org/10.1021/acsomega.3c05263
ACS Omega 2023, 8, 34120−34133

lands) at room temperature (25 °C). Data collection was carried out using Cu K_α radiation (1.5418 Å; 40 kV, 30 mA) as the X-ray source in a 2θ continuous scan mode (Bragg−Brentano geometry) in the range of 5−50° at a scan rate of 1° min^{-1} and a time of 0.5 s/step. The XRD patterns were plotted and analyzed using X'Pert HighScore Plus software.

2.4. Thermal Analysis (DSC/TGA). Differential scanning calorimetry (DSC) of the ALO and ALO−OXA/MLE (salt hydrates) ground mixtures was recorded by using DSC-4000 (PerkinElmer, USA). First, 2−3 mg of each sample was placed in a crimped and non-hermetic aluminum sample pan and run at a heating rate of 10 °C/min in the temperature range of 30−400 °C under a continuous purged dry nitrogen gas flux of 20 mL/min. TGA-4000 (PerkinElmer, USA) was used to measure thermogravimetric analysis (TGA) of the samples. The synthesized salts (<5 mg) were put in a ceramic crucible and heated from 30 to 400 °C used at 10 °C/min under a continuous purged dry nitrogen gas flux of 20 mL/min. All the data were analyzed by using Pyris manager software.

2.5. Scanning Electron Microscope (SEM) Imaging. Mini desktop SEM (ALFATECH-SNE-3200M) is equipped with a BSE detector operating at 5−30 KV. The magnification 60kX with ∼15 nm resolution was employed to identify the morphology of the powder solid forms of ALO salts. A minimum amount of ALO−OXA/MLE salt hydrates (powder) was uniformly dispersed on an adhesive conductive carbon tape and loaded into the SEM chamber and evacuated to high vacuum. A focused beam of electrons was allowed to scan across the sample surface. The images were built by emitted secondary electrons pixel-by-pixel.

2.6. Structure Determination by Powder XRD (SDPD). The crystal structure of ALO−MLE salt hydrate (1:1:1) was solved with the use of powder XRD data measured at room temperature on the Guinier-Huber camera G670 with a curved germanium monochromator (Cu $K_{\alpha 1}$ radiation). The XRD pattern demonstrated the presence of a few characteristic peaks of the ALO. After removing these relatively weak intense peaks from consideration, all the rest peaks were indexed in the monoclinic unit cell. The crystal structure was solved in the space group $P2_1/n$ with the use of the simulated annealing technique.[28] The final bond-restrained Rietveld refinement was performed with the program MRIA[29] following the known procedure described by us earlier.[30] Two crystalline phases were taken into account, namely, ALO and ALO−MLE salt hydrate. For ALO, the atomic coordinates were fixed to the known values taken from the CCDC (refcode ALOPUR). For ALO−MLE salt hydrate, except for the atomic coordinates, only three independent U_{iso} values for non-H atoms were refined—one common U_{iso} for the ALO cation, another one for the monomaleate anion, and the third one for the water oxygen (O6). H atoms were placed in the calculated positions and not refined. The experimental and calculated diffraction profiles after the final two-phase bond-restrained Rietveld refinement are shown in Figure S3, SI.

The ALO−OXA salt hydrate (2:1:0.4) sample was measured on a PANalytical X'Pert Pro powder X-ray diffractometer using non-monochromated Cu K_α radiation in the 2θ range of 6−90°. After the measurements with a step of 0.002°, the raw data were binned to the experimental pattern with a step of 0.01°, which was used in the SDPD analysis. All the observed peaks were indexed in the triclinic unit cell with a volume of 704 $Å^3$. The crystal structure was solved in the space group P-1 with the use of the simulated annealing technique.[28] A careful inspection of the Fourier difference map after preliminary refinement allowed us to find the traces of the disordered water molecule. In the final bond-restrained Rietveld refinement, performed with the program MRIA,[29] only three independent U_{iso} values for non-H atoms were refined—two common U_{iso} for two ALO cations and the third one for the OXA dianion. For the disordered water oxygen O1w, the U_{iso} was fixed to 0.1 and the s.o.f. was refined to 0.421(18). H atoms were geometrically positioned and refined using a "riding model". Surprisingly, H atoms attached to the disordered O1w were not located and left as it is. The observed anisotropy of diffraction-line broadening was approximated by a quartic form in *hkl*.[31] The texture was taken into account with the use of symmetrized harmonics expansion.[32,33] The experimental and calculated diffraction profiles after the final bond-restrained Rietveld refinement are shown in Figure S4, SI. The diffraction data collection, refinement parameters, and geometric parameters of H-bonding for ALO−MLE and ALO−OXA salt hydrates can be found in CIF. The final CIF files (CCDC 2222550 and 2222551) are available in the ESI.

2.7. Energy Calculation. The computational method had been implemented to examine the stability of the ALO salt hydrates compared to the native drug. The crystal structures (CIF files) of ALO, ALO−OXA, and ALO−MLE salt hydrates were optimized within the framework of the density functional theory (DFT) method.[34] The Gaussian 09 program package[35] retaining Becke's three-parameter (Lee, Yang, and Parr (B3LYP)) functional[36−38] along with the 6-31G(d,p) basis set was utilized to calculate the ground state optimized energy and compared their stability aspects.[39]

2.8. Solubility, Dissolution, and Diffusion Study. To determine the solubility of ALO and its salt hydrates in a pH 6.8 phosphate buffer medium, the shake flask method was employed by slurring 200 mg of ALO and its equivalent salts in a 25 mL pH 6.8 phosphate buffer medium for 4 h at 30 ± 2 °C. The standard curve (slope of the absorbances vs concentration of five solutions) was used to determine the absorption coefficients of ALO and its salts at λ_{max} 254 nm by using a UV−vis spectrophotometer.

To obtain the powder dissolution profile of ALO and its salt hydrates, United States Pharmacopeia (USP) dissolution apparatus II (paddle method) was employed on an Agilent 708-DS dissolution tester. ALO (250 mg) and its corresponding salts were ground into a homogeneous mixture and sieved through standard mesh sieves of 200 μm. Each of the powder forms was added into a 60 mL pH 6.8 phosphate buffer medium at 37 °C. The dissolution experiment was continued up to 4 h with a paddle rotation speed of 200 rpm. The aliquots were collected at regular time intervals of 0.5, 1, 2, and 4 h and filtered through a 0.45 μm nylon filter, and corresponding absorbances (concentration) were measured.

In vitro diffusion/permeability studies were carried out using a Franz immersion cell on an Agilent diffusion cell enhancer. ALO (250 mg) and its equivalent salts were suspended with 2 mL of buffer solution in the immersion cell (donor compartment). An artificial dialysis membrane-110 (HiMedia, Mumbai) with an effective surface area of 3.8 cm^2 was kept above the suspension and sealed with the lid. This cell was immersed into the vessel with 60 mL pH 6.8 buffer media. The diffusion experiment was carried out for 6 h with a paddle speed of 200 rpm at 37 ± 1 °C. The aliquot (1 mL) was withdrawn at particular time intervals, and their absorbances were measured at 254 nm using a UV−vis spectrophotometer.

https://doi.org/10.1021/acsomega.3c05263
ACS Omega 2023, 8, 34120−34133

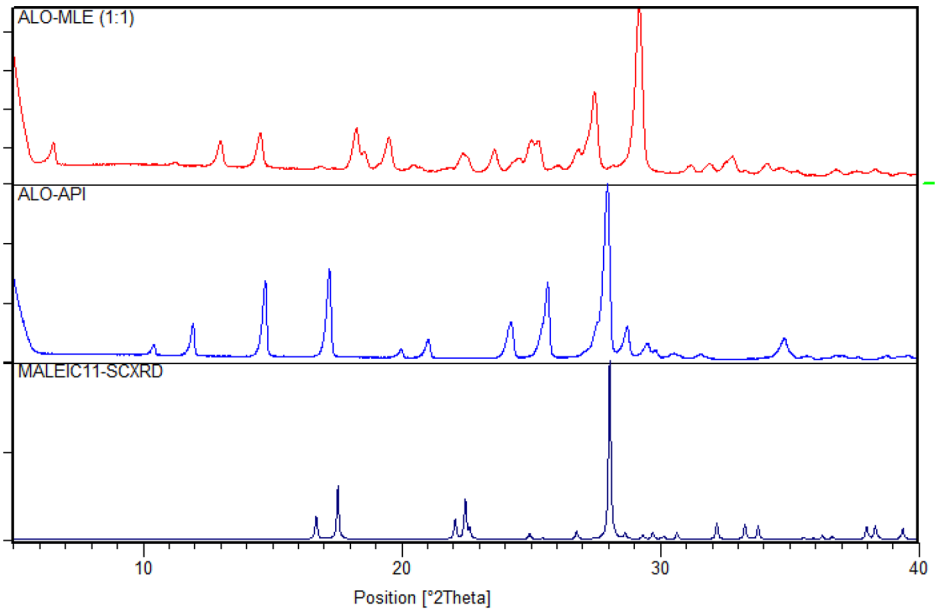

(a)

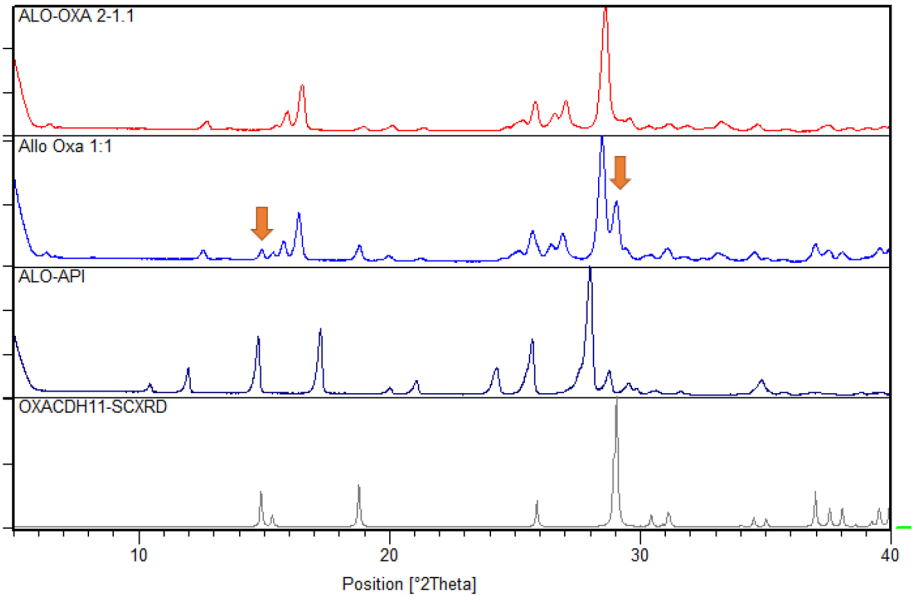

(b)

Figure 2. XRD comparison of (a) ALO−MLE and (b) ALO−OXA with ALO and their acidic coformers (OXA/MLE) confirming the formation new multicomponent phases. Note that ALO−OXA (1:1) had an impurity of OXA peaks that was nullified in ALO−OXA (2:1).

2.9. Pharmacokinetic Study. ALO and its salts were examined for its pharmacokinetic profile in four healthy female BALB/c mice (n = 2 per group, weighing 25−30 g) following oral administration of 30 mg/kg dose. Oral suspension using 0.5% w/v hydroxypropyl methylcellulose with 0.1% (w/v) Tween 80 in water was administered. After dosing, 50 μL of blood samples was collected from the saphenous vein at 0.5, 1, 2, 4, 6, and 24 h from each mouse. The plasma was segregated by centrifugation at 3500 rpm for 10 min at 4 °C and stored at −80 °C until further analysis. The plasma concentrations of the ALO and its salts were determined by a validated UPLC-MS/MS method.[40] The pharmacokinetic parameters (e.g., maximum plasma concentration (C_{max}), time to achieve this (T_{max}), area under the curve 0−24 h (AUC_{0-24}), and half-life ($T_{1/2}$)) were calculated using the PK solver tool and reported as mean and standard deviations.

2.10. Moisture and Thermal Stability. To access the moisture effect on the ALO salts, the drug and salts were exposed in a closed desiccator, maintaining a temperature of 30 ± 5 °C and 75 ± 5% relative humidity for 2 months. The phase changes were monitored by PXRD every week. In addition, the ALO and its salts were exposed at 60 and 110 °C in an oven for an hour and monitored their phase transformation using PXRD to gain its thermal stability profile.

https://doi.org/10.1021/acsomega.3c05263
ACS Omega 2023, 8, 34120−34133

3. RESULTS AND DISCUSSION

ALO is a weak base (pK_a 10.1) in which pyrimidine sp^2 nitrogen as the most potent electron pair donor is expected to form neutral/ionic hydrogen bonds with the acidic coformers. This was confirmed by the reported crystal structure of chloride (CCDC refcode FAXFUF10) and sulfate (refcode OGEREY) salts[21,22] and cocrystals with pyridine 2,4-dicarboxylic acid (pK_a 2.15),[23] 2,4-dihydroxybenzoic acid (pK_a 3.1, 8.5), and isonicotinamide.[24] These multicomponent solids suggest that coformers should be stronger carboxylic acid (pK_a <2) compared to the reported acidic coformers to produce organic molecular salts of ALO. To overcome the poor aqueous solubility and permeability of ALO, the drug was cocrystallized with several di-/tricarboxylic acids, amides, and amino acids that resulted in new solid phases with oxalic acid (pK_a 1.2, 4.2) and maleic acid (pK_a 1.9, 6.1). Table S1 summarizes the complete list of coformers used during ALO cocrystal/salt screening. The ΔpK_a (pK_a of ALO − pK_a of acid) of ALO−MLE and ALO−OXA are greater than 8, which indicates the high possibility of salt formation.[10] The new multicomponent ALO−MLE/ALO−OXA phases were confirmed by XRD, DSC, TGA, and FT-IR data. Surprisingly, both the ALO−MLE and ALO−OXA salts crystallized as ALO during crystallization irrespective of solvents and crystallization methods. Crystallization of ALO salts in mixed solvents like MeOH−water, EtOH−water, and 2-PrOH−water via slow evaporation always rendered the acicular morphology of ALO crystals (confirmed with SCXRD). Fast evaporation, anti-solvent crystallization, and layer crystallization also did not give the expected outcome. In addition, crystallization at 50 °C (hot plate) and 5 °C (freezer) resulted in ALO crystals only. Factors such as the thermodynamic stability of the ALO crystal and the difference between the aqueous solubility of ALO and the coformers OXA/MLE are the probable reason behind the difficulty to produce the single crystal. Hence, the crystal structures of these new multicomponent solid phases were solved using Rietveld refinement from the high-resolution PXRD data.

3.1. PXRD Analysis. ALO extraction from the commercial Zyloprim tablets resulted in a white crystalline material. The XRD pattern of the extracted ALO and pure ALO (from Lupin Ltd.) was compared with its crystal structure (CCDC refcode ALOPUR) reported in the Cambridge Structural Database (CSD).[41] The characteristic diffraction peaks of ALO at 10.4, 12.0, 14.8, 17.2, 24.3, 25.8, and 27.9 ± 0.2° 2θ matched that confirmed the purity of the drug (refer Figure S1, SI). As expected, the extracted crude ALO showed a slightly broad diffraction pattern compared to the pure drug due to anti-solvent crystallization. The novelty of ALO−MLE (1:1) was confirmed using the XRD diffraction peaks, which are characteristic when compared with that of ALO and MLE. ALO−MLE showed distinct diffraction peaks at 6.5, 13.0, 14.5, 18.3, 19.5, 20.5, 23.6, 27.4, and 29.2° ± 2θ (Figure 2a) that confirmed a new binary solid phase. Similarly, ALO−OXA (1:1) ground materials exhibited a new XRD pattern at 6.3, 12.7, 15.9, 16.5, 26.6, 27.0, and 28.6° ± 0.2° 2θ along with a few shoulder diffraction peaks at 14.9 and 29.0 ± 0.2° 2θ that corresponds to the coformer oxalic acid dihydrate (refer Figure 2b). Comparatively, the ALO−OXA (2:1) ground mixture diminished the diffraction peaks corresponding to OXA dihydrate and exhibited a comparatively pure binary solid (Figure 2b). The XRD result of ALO−MLE (1:1) indicates that MLE, however it is a dicarboxylic acid, may have intramolecular hydrogen-bonded carboxylic acid in which one carboxylic acid is only available to form a hydrogen-bonded complex with ALO. In the case of ALO−OXA (2:1), OXA may use both the carboxylic acids for hydrogen bonding with ALO.

3.2. Thermal Analysis. DSC of a solid phase confirms the exact melting point, degradation, and phase transformation, whereas TGA indicates water/solvent loss and stability/degradation with an increase in temperature. ALO melted at 385−390 °C, whereas both ALO−MLE and ALO−OXA exhibited characteristic melting points when compared with the corresponding API and acidic coformers. ALO−MLE (hydrate) exhibited a dehydration onset at 106.9 °C and a melting onset at 146.6 °C that suggest that the binary phase melted in between the melting points of ALO and MLE (135 °C). Following melting, ALO−MLE (hydrate) decomposed to ALO that exhibited a broad melting endotherm in the range of 380−390 °C. The broad endotherm of ALO−MLE within 115 °C indicates a possibility of dehydration, which was further confirmed by the 6.6% weight loss in TGA data. The theoretical weight loss of 1 equiv of water per ALO−MLE was 6.6%, which concords with the experimental weight loss (refer Figure 3a). Further, the DSC profile of ALO−OXA (hydrate) showed a very broad endotherm (dehydration) in the temperature range of 113−139 °C and a melting onset at 217 °C, which is intermediate between the m.p. of ALO and OXA (189 °C). ALO−OXA (hydrate) finally decomposed to ALO at 375.4 °C. The TGA data of ALO−OXA also supported a weight loss of 1.8% up to 170 °C that corresponds to a 0.4 water molecule (refer Figure 3b). This weight loss can be concluded as a nonstoichiometric amount of water (<1 equiv)[42,43] present in ALO−OXA. DSC/TGA thermograms further confirmed the thermal stability of ALO−OXA (hydrate) compared to ALO−MLE (hydrate).

3.3. Vibrational Spectroscopy Analysis. Vibrational spectroscopy indicates the functional groups present by measuring the asymmetric stretching/bending vibrations of a compound. In addition, this is a powerful tool to predict whether ionization (salt form) occurs or not during an acid−base reaction. ALO consists of a multiple number of hydrogen-bonded donors (2) and acceptors (3) that offer variable interactions when forming multicomponent solids with complementary functional groups, e.g., carboxylic acid, as in this study. ALO exhibits amide CO, C=N, and N−H stretching vibrations at 1701, 1575, and 3176 (broad) cm^{-1}, respectively. In the presence of carboxylic acid coformers, e.g., OXA and MLE, vibration frequencies of ALO functional groups changed. Note that MLE and OXA (dihydrate) showed CO vibrations at 1710 and 1654 (broad) cm^{-1}. ALO−MLE (hydrate) exhibited C=O vibrations at 1689 cm^{-1}, C=N vibration at 1485 cm^{-1} (broad), NH stretching at 3120 and 3396 cm^{-1}, and OH stretching at 3529 cm^{-1} (refer Figure 4a). The vibrational frequencies suggest that pyrimidine C=N got protonated and an additional NH peak appeared at 3396 cm^{-1}. In addition, disappearance of the MLE CO vibration further suggests that the possibility of ionized MLE and additional NH vibration confirms the salt hydrate formation. The hypsochromic shift of ALO carbonyl vibration at 1689 cm^{-1} represents the changes in hydrogen bonding during interactions with MLE. Similarly, ALO−OXA (hydrate) exhibited C=O vibrations at 1695 cm^{-1}, C=N vibration at 1562 cm^{-1} (broad), NH stretching at 3113 and 3246 cm^{-1},

https://doi.org/10.1021/acsomega.3c05263
ACS Omega 2023, 8, 34120−34133

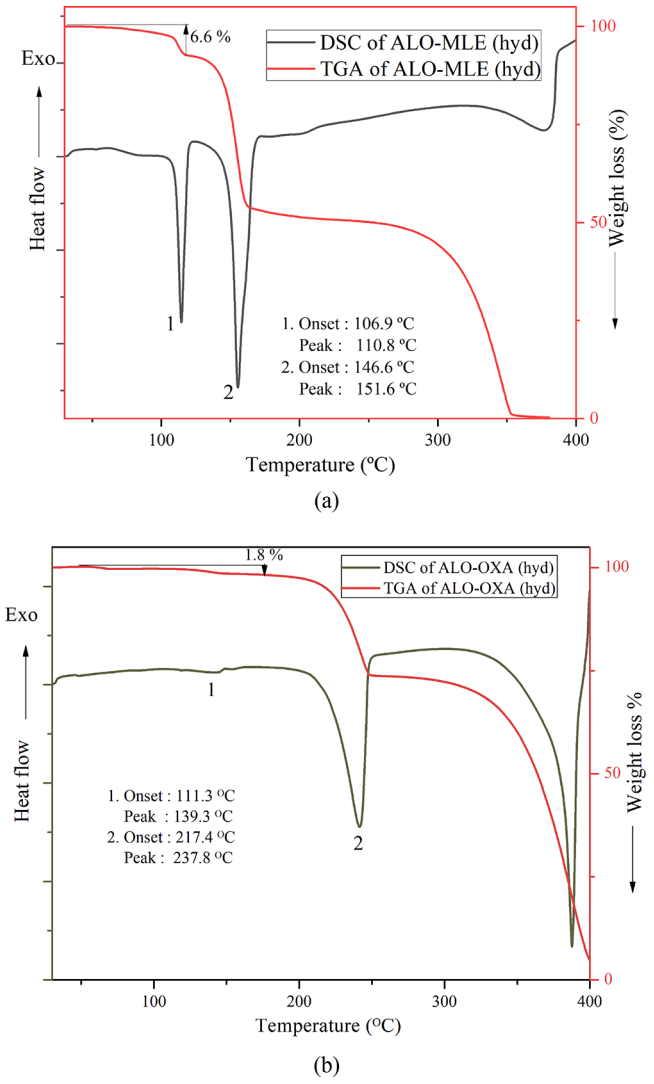

Figure 3. DSC and TGA plot of (a) ALO−MLE hydrate and (b) ALO−OXA hydrate confirming more thermal stability of the latter.

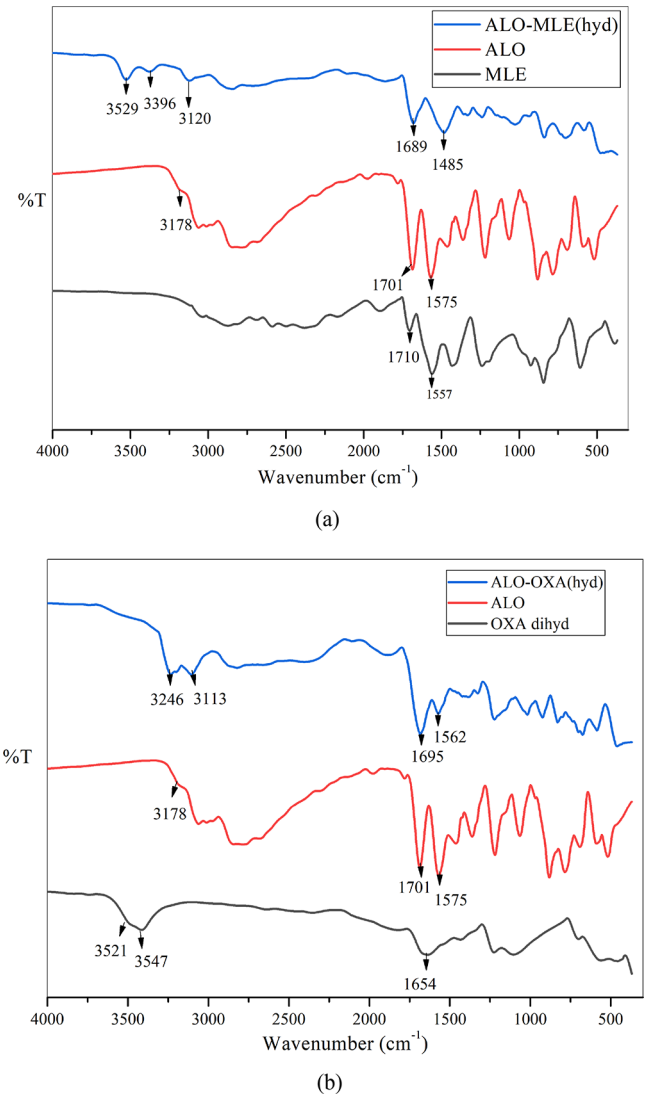

Figure 4. Vibrational spectra of (a) ALO−MLE (hydrate) and (b) ALO−OXA (hydrate) compared to ALO and acid coformers suggesting the possibility of salt hydrate formation.

and OH stretching at 3520 (broad) cm^{-1} (refer Figure 4b). This represents ALO−OXA in an ionized form as an additional NH stretching frequency due to the protonated pyrimidine nitrogen atom and disappearance of the OXA carboxylic acid peak. A minor hypsochromic shift (6 cm^{-1}) suggests that ALO carbonyl may not participate in strong hydrogen bonding with OXA. A very broad OH vibration above 3500 cm^{-1} confirmed the possibility of unbound or nonstoichiometric hydrate in the salt.

3.4. Crystal Structure Analysis. ALO consists of planar pyrimidine and pyrazole-fused rings, and out of them, pyrimidine "N" is more basic that is confirmed with the reported HCl and H_2SO_4 salts.[21,22] In the ALO crystal structure (refcode ALOPUR, $P2_1/c$, Z = 4), two ALO molecules form a N−H···N centrosymmetric dimer between pyrimidine and pyrazole nitrogen atoms[20] (refer Figure S5a, SI). These dimers are extended to another via N−H···N hydrogen bonds and form a 2D sheet along the *bc* plane. ALO-HCl salt (refcode FAXFUF10, *Pnma*, Z = 4)[21] represents the proton transfer from HCl to the pyrimidine sp^2 nitrogen atom that confirmed its ionized state (Figure S5b, SI). The H-bonded centrosymmetric ALO dimer is replaced by the N−H···O hydrogen-bonded catemer. Each Cl anion binds two ALO cations via N^+−H···O^- ionic H-bonds. The overall crystal structure maintains the 2D planar sheet along the *bc* plane. Similarly, in ALO sulfate salt (refcode OGEREY, $C2/c$, Z = 8),[22] a proton is transferred from the sulfuric acid to the pyrimidine "N" of ALO (Figure S5c, SI). Here, also, the ALO dimer is replaced with the N−H···O hydrogen-bonded catemer involving pyrimidine and pyrazole "N" atoms. The ALO cation and sulfate anion are alternatively arranged and form a 2D sheet. Each sulfate anion is strongly bound with five ALO cations via N^+−H···O^- and N−H···O H-bonds using its four oxide anion acceptors.

The idea of synthesizing organic salts of ALO with OXA and MLE was similar to the reported inorganic chloride and sulfate salts that may offer improved solubility and permeability. We faced difficulty to produce single crystals of ALO−OXA and ALO−MLE hydrates irrespective of crystallization methods. Most often, the crystallization resulted in ALO (needle morphology) only. Hence, high-resolution PXRD as an alternative method was availed to determine the crystal structures of these multicomponent solids.[30] The crystallographic parameters of these salts are listed in Table 1.

https://doi.org/10.1021/acsomega.3c05263
ACS Omega 2023, 8, 34120−34133

Table 1. Crystallographic Details of ALO Salts

	ALO−MLE hydrate (1:1:1)	ALO−OXA hydrate (2:1:0.4)
CCDC no.	2222550	2222551
chemical formula	$C_5H_5N_4O^+$, $C_4H_3O_4^-$, H_2O	$2(C_5H_5N_4O)^+$, $C_2O_4^{2-}$, $0.42(H_2O)$
MW	270.212	380.2
crystal system, space group	monoclinic, $P2_1/n$	triclinic, P-1
T (K)	295(2)	295(2)
a (Å)	5.1353(7)	13.6693(11)
b (Å)	27.350(3)	14.4570(12)
c (Å)	8.5532(9)	3.6474(5)
α, β, γ (°)	90, 105.585(14), 90	94.092(12), 93.250(11), 78.439(9)
V (Å^3)	1157.1(2)	703.679
ρ_{calc} (g cm^{-3})	1.551	1.742
μ (mm^{-1})	1.152	1.257
radiation	Cu $K_{\alpha 1}$	Cu K_α
specimen shape, size (mm)	flat sheet, 15 × 1	flat sheet, 15 × 1
θ values (°)	$2\theta_{min}$ = 5.0, $2\theta_{max}$ = 90.0, $2\theta_{step}$ = 0.01	$2\theta_{min}$ = 6.0, $2\theta_{max}$ = 90.0, $2\theta_{step}$ = 0.01
profile	R_p = 0.0289, R_{wp} = 0.0377,	R_p = 0.0214, R_{wp} = 0.0272,
R factors, WR_2, goodness of fit	R_{exp} = 0.0187, GOF =2.020	R_{exp} = 0.0113, GOF = 2.416
method of structure determination	PXRD	PXRD

3.4.1. ALO−MLE Hydrate (1:1:1). The crystal structure of ALO−MLE hydrate was solved in the monoclinic $P2_1/n$ space group, and there is one molecule each of the ALO cation, maleate monoanion, and water molecule in the asymmetric unit. The maleic acid protonates the pyrimidine nitrogen N2 by breaking the centrosymmetric dimer of ALO, thus forming the N^+−H···O^- ionic hydrogen bond [$N2^+$−H3···$O3^-$: 1.72, 2.5582(3) Å, 162°]. Table S2 summarizes the hydrogen-bond geometry of the ALO salts. The salt formation was further confirmed by the equal CO bond distances (1.25/1.26 Å) of the MLE carboxylate anion and the increased endocyclic <C−N−C bond angle of 117.8° from 112° (ALO) involving the protonated pyrimidinium "N" atom. MLE, even though dicarboxylic acid, most often donates one proton only as another proton is involved in the O−H···O^- intramolecular hydrogen bond. In ALO−MLE salt hydrate, the monomaleate anion involves in the O−H···O^- intramolecular ionic hydrogen bond. In addition, the amide NH of ALO also forms a N−H···O^- hydrogen bond (N1−H1···O4: 1.84, 2.7673(4) Å, 168°) with the monomaleate anion. Finally, two ALO cations and two monomaleate anions form a tetramer ring motif of $R_4^4(22)$ using N^+−H···O^- and N−H···O^- hydrogen bonds (refer Figure 5a). In addition, one water molecule forms multiple hydrogen bonds using its two donor hydrogen atoms and one oxygen atom. One water molecule binds two ALO cations via O−H···O (O6−H6A···O1: 1.88, 2.8379(4) Å, 177°) and N−H···O (N3−5H···O6: 1.99, 209515(4) Å, 169°) hydrogen bonds involving pyrimidine carbonyl and pyrazole NH. Further, the water molecule acts as a second donor to the monomaleate anion and forms an O−H···O^- hydrogen bond. In fact, there are two molecules each of ALO cations, MLE monoanions, and water molecules form the hexamer ring motif of $R_8^8(30)$ (refer Figure 6b). These hexamers are extended to the next tetramer through water molecule as a bridge. Needless to mention, this water molecule is strongly hydrogen bonded with two ALO cations and one MLE anion that predicts the excellent stability of the salt hydrate at ambient conditions. In addition, water molecules dictate the zigzag pattern of the H-bonded complex when viewed down the a-axis (Figure 5c). The supramolecular assembly of the salt structure is further stabilized by multiple auxiliary interactions (e.g., C−H···O, C−H···N, and $\pi\cdots\pi$ stacking interactions).

3.4.2. ALO−OXA Hydrate (2:1:0.4). The crystal structure of ALO−OXA hydrate was solved in the triclinic P-1 space group with two ALO cations, one oxalate anion, and one non-stoichiometric water molecule (s.o.f. 0.4) in the asymmetric unit. Unlike maleic acid in ALO−MLE salt hydrate, here, oxalic acid as dicarboxylic acid donates both the protons to 2 equiv of ALO and forms ALO−OXA salt hydrate. The salt formation was confirmed by the similar CO bond distances (1.24/1.27 Å) of the OXA anion and the increased endocyclic <C−N−C bond angle of 117.8 and 118.1° from 112° (ALO) of the protonated pyrimidinium "N" atom. The OXA dianion protonates the pyrimidine nitrogen N1A/B of ALO cations by forming bifurcated N^+−H···O^- charge-assisted hydrogen bonds ($N1A^+$−H1A···$O2^-$: 2.51, 3.0647(4) Å, 123°; $N1A^+$−H1A···$O3^-$: 2.08, 2.9004(4) Å, 160°; $N1B^+$−H1B···$O1^-$: 2.23, 3.0632(4) Å, 162°; $N1B^+$−H1B···$O4^-$: 2.41, 3.0078(4) Å, 127°) (refer Figure 6a). Two ALO conformers (cations) and one OXA anion form a trimer of the $R_3^2(10)$ ring motif via N−H···O (N4A−H5A···O1B: 2.15, 2.9302(4) Å, 151°) and N−H···O^- (N1B−H1B···O1: 2.23, 3.0632(4) Å, 162°; N2A−H3A···O1: 1.83, 2.6330(4) Å, 155°) hydrogen bonds. This trimer is extended to another trimer via N^+−H···O^- ionic H-bonds forming the hexamolecular assembly of the ring $R_6^6(28)$ motif involving four ALO cations and two OXA anions. In addition, one OXA anion forms four ionic N^+−H···O^- hydrogen bonds from the surrounding four ALO cations. Two ALO cation conformers are intermolecularly hydrogen bonded via N−H···N interactions (N3B−H5B···N3A: 1.90, 2.7053 Å, 156°) involving imidazole nitrogen atoms, which are absent in the crystal structure of ALO and ALO−MLE salt hydrate. Further, four ALO cations form N−H···N and N−H···O hydrogen-bonded tetramers of the $R_4^4(18)$ ring motif that suggests the possibility of the second form of ALO. Interestingly, the water molecule is only bound with the carbonyl acceptor of ALO cations, not with the OXA anion (refer Figure 6b). Two water molecules occupy in the cavity formed by the ALO tetramers. Here, water molecules, apart from the H-bond with the carbonyl acceptor of the ALO cation, form a hydrogen-bonded water chain along the c-axis (Figure 7c). In addition, the auxiliary interactions (e.g., C−H···O and $\pi\cdots\pi$ stacking interactions) stabilized the supramolecular assembly of the ALO−OXA salt hydrate. The crystal density (1.742 g cm^{-3}) of ALO−OXA hydrate indicates very dense packing of its crystal structure.

Generally, the architecture of a cocrystal/salt is often dependent on the interactions associated with the parent drug, and thus, the stoichiometry of the constituting components is designed accordingly. Often, experimental conditions also govern the formation of specific stoichiometric products.[15,44] Salts are more prone to hydrate formation due to better packing efficiency and hydrogen-bonding aspects of the water molecule compared to the cocrystal. Almost one-third of the commercial drugs are formulated as hydrates.[45] Hydrates can be classified into stoichiometric (where drug:water is defined but not necessarily an integer number) and non-stoichiometric (variable number of water molecules incorpo-

https://doi.org/10.1021/acsomega.3c05263
ACS Omega 2023, 8, 34120−34133

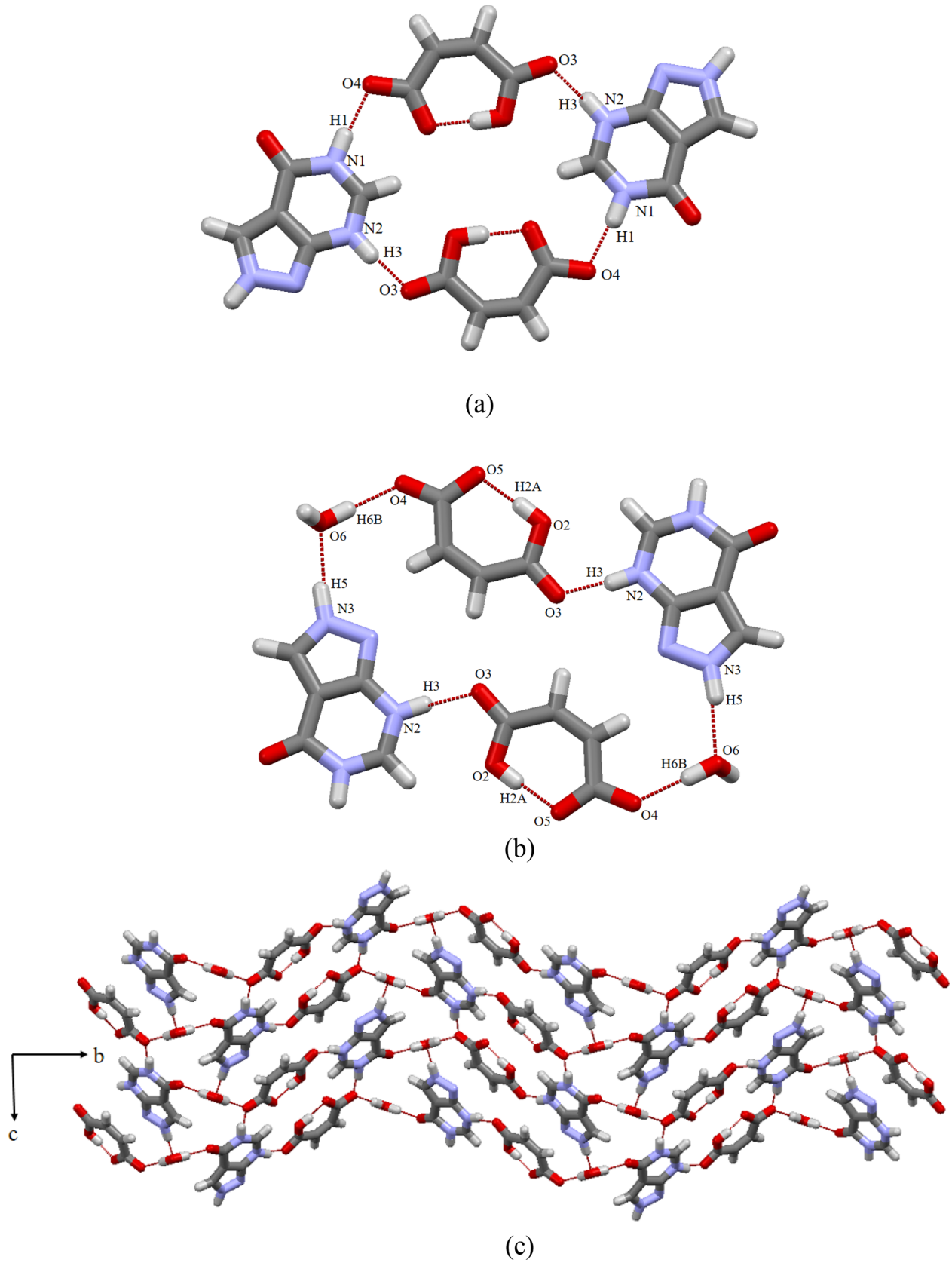

Figure 5. (a) Hydrogen-bonded tetramer between the ALO cation and the MLE anion in ALO−MLE salt hydrate. (b) Hexamer ring motif in ALO−MLE salt hydrate. (c) Water molecule directed zigzag pattern of the salt when viewed down the *a*-axis.

rated in a crystal lattice).[46,47] Nonstoichiometric hydrates are generally observed when the water molecules occupy in the voids/channels in the crystal lattice rather than involving in direct hydrogen bonding. As a result, water molecules may

https://doi.org/10.1021/acsomega.3c05263
ACS Omega 2023, 8, 34120−34133

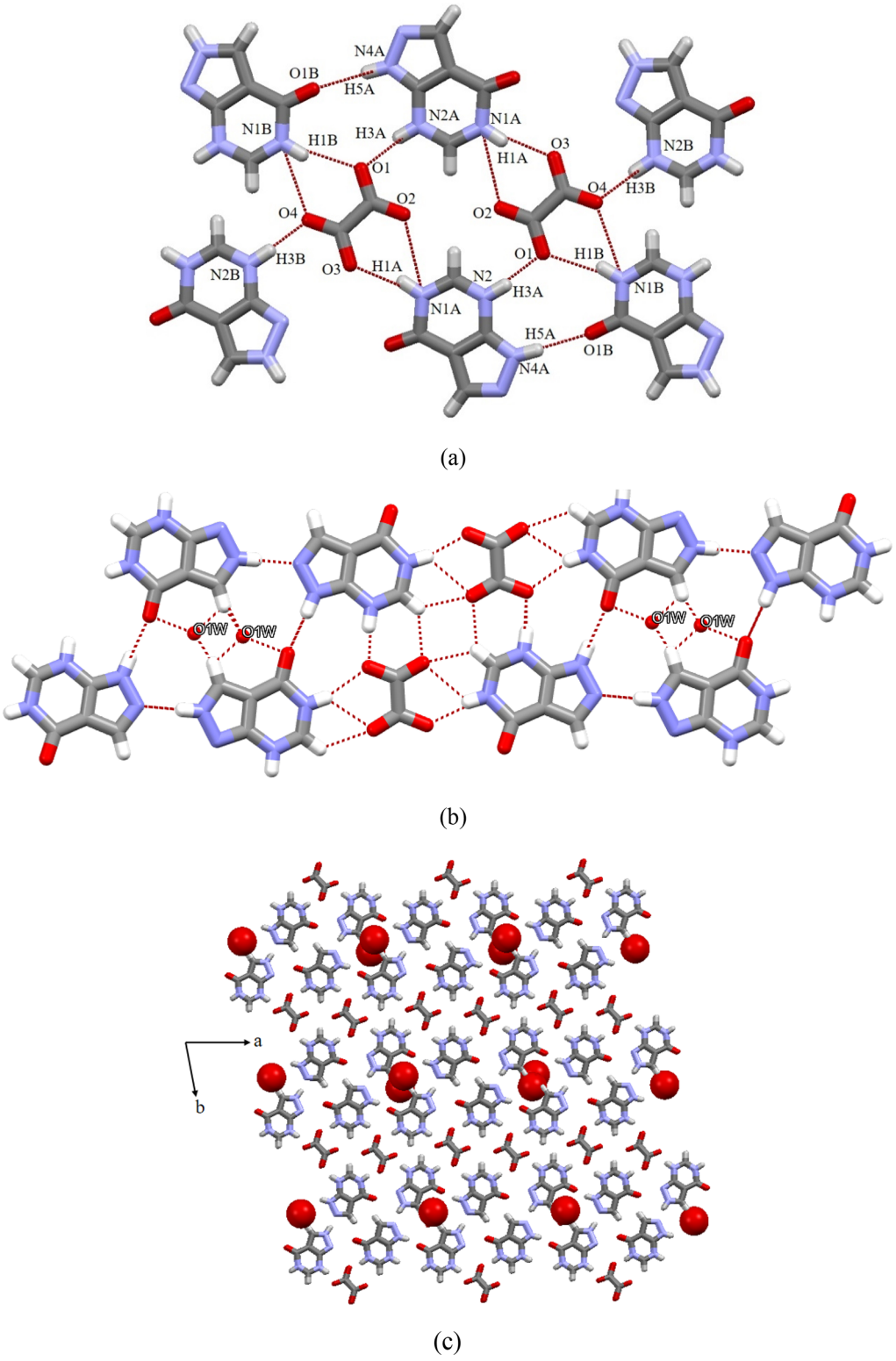

Figure 6. (a) Hydrogen bonding in ALO−OXA (2:1:0.4) salt hydrate. (b) Nonstoichiometric water (s.o.f. 0.42) molecule forming an H-bond to carbonyl of the ALO cation and residing in the cavity of ALO tetramers. (c) Packing of ALO−OXA salt hydrate, wherein water molecules form a zigzag chain when viewed down the *c*-axis.

fully or partly escape through these channels without significant changes in the crystal structure. In other cases, these water molecules interact with other water molecules, although intervening drug molecules are considered as isolated site hydrates. Nonstoichiometric hydrates are generally difficult to manage as the water molecules are either loosely bound or interact with other water molecules present in the channel. As a result, uses of nonstoichiometric hydrate may compromise with the drug properties (e.g., stability). Sitagliptin L-tartrate hemihydrate (2:2:1) is an example of both stoichiometric and nonstoichiometric hydrates as following dehydration the salt retained its crystal structure.[46] The sodium salt hydrates of

https://doi.org/10.1021/acsomega.3c05263
ACS Omega 2023, 8, 34120−34133

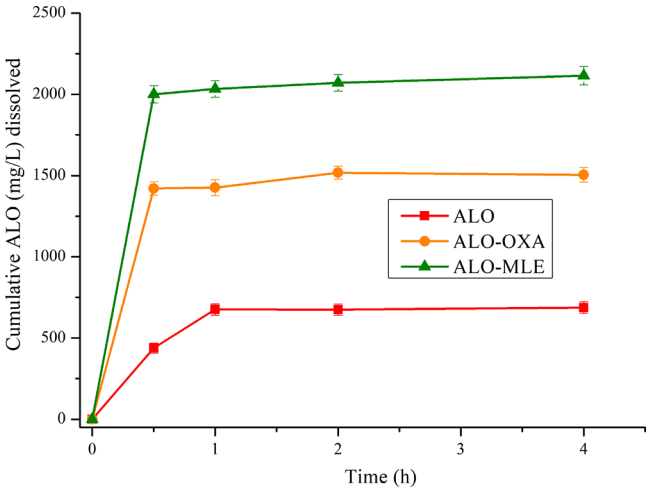

Figure 7. Dissolution profile of ALO and its salts in pH 6.8 phosphate buffer at 37 °C.

cromolyn and cefazolin are examples of nonstoichiometric channel hydrates that showed anisotropic lattice contraction during dehydration experiments.[47] In this context, ALO−OXA hydrate (2:1:0.4) salt is an example of nonstoichiometric hydrate, whereas ALO−MLE salt hydrate (1:1:1) consists of stoichiometric water. Note that both ALO−OXA and ALO−MLE salt hydrates are exceptionally stable during storage at ambient conditions due to strong neutral/ionic hydrogen bonding with the drug (cation) and carboxylate.

3.5. Solubility and Dissolution Studies. Solubility and dissolution play a vital role in determining the absorption and bioavailability of a drug.[13,48−50] ALO exhibits poor aqueous solubility. The dense packing of ALO molecules in its crystal structure, strong hydrogen-bonded dimer/hexamer involving pyrimidine/pyrazole ring "N" atoms, and exceptionally high melting point are the probable reason for its poor solubility. Since the drug has ionizable pyrimidine/pyrazole moieties, salts were prepared with the comparatively stronger carboxylic acids MLE and OXA to enhance its solubility. Solubility experiments of ALO and its salt hydrates were carried out in a neutral phosphate buffer (pH 6.8) medium to estimate the advantage of these ionized solid forms without altering the pH of the medium. Note that OXA and MLE, being aliphatic dicarboxylic acids, did not interfere in the λ_{max} of ALO at 254 nm [λ_{max} (MLE) 210 nm and λ_{max} (OXA) 214 nm] during the estimation of solubility using a UV−vis spectrophotometer. After 4 h of solubility experiments, ALO−MLE salt hydrate demonstrated the highest solubility of 2115 mg/L when compared to ALO−OXA hydrate (1504 mg/L) and native drug ALO (687 mg/L). Solubility data indicates that salt hydrates exhibited 2−3-fold improved solubility compared its native drug; however, both the salts transformed to ALO during the solubility experiments, confirmed with XRD data (Figure S6, SI).

To determine the apparent solubility gained by the ALO salts before phase transformation, dissolution experiments of ALO and its salts were carried out in a pH 6.8 phosphate buffer medium at 37 °C. The result showed that the ALO salts attained the maximum solubility (ALO−MLE hydrate, 2001 mg/L; ALO−OXA hydrate, 1426 mg/L) within 0.5 h, followed by saturation of solubility (plateau region) up to 4 h of the dissolution experiment. ALO salts achieved maximum apparent solubility until they dissociated. Following dissociation of the salts, ALO cations remain in the solution phase up to a certain extent that favors higher dissolution compared to the native drug. Note that the pH of the buffer medium was maintained in range of 6.6 to 6.8 during the dissolution experiment. Comparatively, ALO gained maximum solubility (676 mg/L) at 1 h of the dissolution experiment. Table S3 summarizes the kinetic solubility data of ALO and its salts during dissolution experiments. ALO salt hydrates enhanced apparent solubility by 3.2−4.6-fold within 30 min of the dissolution experiment (refer Figure 7). Both the salt hydrates converted to pure API within 2 h of the dissolution experiment (see Figure S7, SI). Generally, salts exhibit excellent solubility compared to their native drug due to the ionization effect and increased polarity/wettability in the solution. The improved solubility of ALO−MLE (hydrate) compared to ALO−OXA (hydrate) and ALO can be correlated based on the ionization, lower melting point of the salts, and higher solubility of the MLE/OXA coformer. Note that the aqueous solubilities of MLE and ALO are 788 and 143 g/L. Generally, the solubility of a multicomponent solid increases with an increase in the proportion of the soluble coformer. ALO−MLE hydrate (1:1:1) has 1 equiv of MLE per 1 equiv of drug, whereas ALO−OXA hydrate (2:1:0.4) has 0.5 equiv of OXA.

On the structural point of view, the ALO cation and MLE anion form alternate hydrogen bonds in the corresponding ALO−MLE salt hydrate, whereas ALO−OXA salt hydrate maintains the tetramer ring of ALO only. This suggests that the ALO−OXA salt (hydrate) crystal structure is close to that of ALO. In fact, OXA anions are strongly bound with the tetramer assembly of ALO cations that resists the OXA molecule to close in contact with the aqueous medium. In addition, ALO−MLE salt hydrate forms a zigzag network, whereas ALO−OXA (hydrate) salt maintains the planar sheet similar to the ALO crystal structure. To summarize, ALO−MLE (hydrate) salt is able to modify the overall structure pattern, whereas ALO−OXA (hydrate) salt maintains partially similar to the crystal structure of ALO that is the probable reason behind the improved dissolution/solubility of ALO−MLE (hydrate) compared to ALO−OXA (hydrate) salt. In addition, ALO−OXA hydrate (1.74 g/cc) exhibits denser crystal packing compared to ALO−MLE salt hydrate (1.55 g/cc) (refer Table 1).

3.6. In Vitro Diffusion Studies. Semipermeable membranes are commonly used during drug discovery and development to access the passive diffusion of orally administered drug molecules. It can provide basic information about a drug's ability to cross the hydrophobic biological barriers, such as the mucous membrane and blood−brain barrier. Generally, the Caco-2 monolayer, human epithelial cell, porcine skin, rat skin, and semipermeable membranes like PAMPA membrane, dialysis membrane, cellulose nitrate, Cuprophan, polymethylsiloxane, Permeapad barrier, and silicon are used in a Franz diffusion cell to access the in vitro diffusion profile of a drug.[8] The synthetic membranes are commonly used when biological skin is not readily available. Dialysis membranes are easily accessible and recent literature discussed on its applications toward tuning diffusion of drugs.[7,14] ALO demonstrates poor solubility and permeability, which needs an urgent remedy. Solubility and intestinal permeability are the essential parameters for a drug to govern its bioavailability.[13,50] The diffusion rate (flux) of a drug depends upon the concentration gradient, lower crystal density, and weaker non-covalent interactions between two

https://doi.org/10.1021/acsomega.3c05263
ACS Omega 2023, 8, 34120−34133

components in a multicomponent solid.[7,14,24] Hence, a drug with higher solubility may diffuse better through the dialysis membrane. These higher-soluble ALO salt hydrates will have the positive impact on the diffusion permeability of ALO. To examine the diffusion behavior in neutral pH 6.8 buffer media using an artificial semipermeable dialysis membrane (sheet of regenerated cellulose), powder samples of ALO and its OXA/MLE salts in the (buffer) wet granule phase were placed in the donor chamber of a Franz diffusion cell and allowed to diffuse to the acceptor chamber through the intermediate dialysis membrane at 37 ± 0.5 °C. The aqueous samples in the acceptor compartment were periodically withdrawn in specific time intervals to determine the concentration of the diffused ALO and diffusion rate. Diffusion studies of ALO salts also follow the similar pattern as the dissolution profile wherein ALO−MLE salt hydrate maintained its superior diffusion properties compared to ALO−OXA salt hydrate and the native drug (refer Figure 8a). The improved dissolution/solubility of the ALO−MLE hydrate salt increased the concentration gradient in the donor chamber that facilitates more diffusion of the drug through the dialysis membrane. Surprisingly, the diffusion of the ALO−MLE salt hydrate continued to increase steadily even after 6 h of the experiment. The cumulative drug diffusion rates of ALO−MLE and ALO−OXA hydrates are 7.6 and 3.7 mg/cm^2 compared to the native drug (0.61 mg/cm^2) at 6 h that indicates the superior diffusion of the ALO−MLE (12.4-fold) and ALO−OXA (6.0-fold) salt hydrates. Figure 8b represents the diffusion rate (flux, mg/cm^2/h) vs time plot that indicated that the flux of ALO increased instantly within 15−30 min, followed by a gradual fall in the rate. ALO−MLE salt (hydrate) exhibited the highest flux of 2.8 mg/cm^2/h at 30 min of diffusion experiments, whereas ALO−OXA salt (hydrate) maintained an intermediate flux (0.69 mg/cm^2/h) between the ALO−MLE salt hydrate and native drug. Table S4 summarizes the diffusion data including the flux of ALO and its salts for comparison purposes. Following the completion of the diffusion studies, both salts converted to ALO, which was confirmed by using PXRD. The crystal density of ALO (1.635 g/cc), ALO−OXA hydrate (1.742 g/cc), and ALO−MLE hydrate (1.551 g/cc) suggests that ALO−MLE salt hydrate exhibits comparatively loose packing and higher solubility that permits ALO to increase thermodynamic activity and thus release the drug faster than ALO and ALO−OXA salt (hydrate). In addition, MLE is more lipophilic due to the presence of olefin carbons compared to OXA that assist further to diffuse the drug more through the hydrophobic membrane. Moreover, the irregular morphology (SEM images; Figure S8, SI) with a higher surface area/lower aspect ratio of the ALO−MLE and ALO−OXA salt hydrates compared to the rod-like ALO crystals demonstrates the advantages of the ALO salt hydrates in terms of dissolution/diffusion properties.

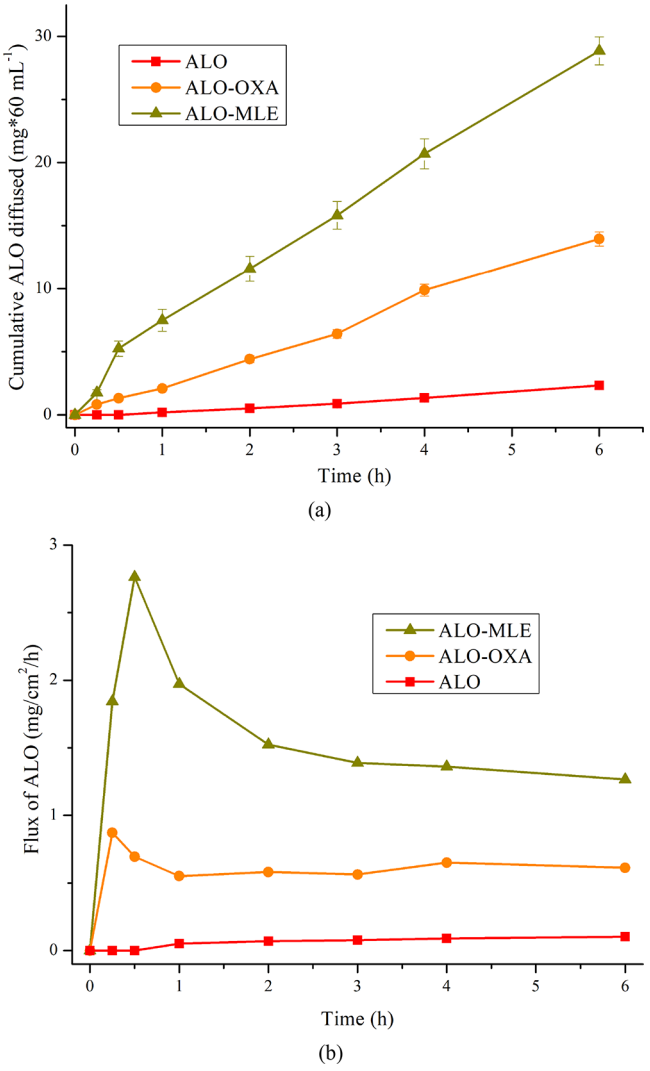

Figure 8. (a) Diffusion plot and (b) flux of ALO and its salts with respect to time demonstrating the advantage of ALO−MLE in improving its diffusion properties.

The ground state energy calculation is used to determine the lowest possible energy state of a quantum mechanical system. DFT calculations using B3LYP and 6-31G(d,p) basis set suggest that the ground state optimized energies of ALO, ALO−OXA (hydrate), and ALO−MLE (hydrate) are −486.90, −1351.95, and −1018.81 Hartree, respectively. Hence, the stability order among the three solid forms is ALO < ALO−MLE (hydrate) < ALO−OXA (hydrate). The energy calculation suggests that ALO−OXA hydrate (2:1:0.4) is a more stable hydrogen-bonded complex with stronger non-covalent (ionic) interactions compared to ALO−MLE hydrate (1:1:1) and ALO. Accordingly, ALO−MLE salt (hydrate) dissolved and diffused more drugs compared to ALO−OXA salt (hydrate) during dissolution and diffusion studies following the collapse of the corresponding ionic hetero-synthon, which is also explained in terms of structure correlation and thermal behavior. The energy of the salts will be lowered due to the ionic bond formation, which induces ion−dipole interactions in the solution state by releasing energy. This energy can lower the overall energy of the system. The higher energy of ALO can be attributed to high electron density (Hohenberg−Kohn theorem)[51] and neutral hydrogen bonds involved in its crystal structure. Thus, the non-ionizable ALO exhibits higher energy when compared to its organic salts.

3.7. Pharmacokinetic Evaluation. Bioavailability refers to the fraction of a solid dosage form that remains active until it reaches the target biological site of action. Most of the orally administered APIs struggle to maintain its 100% (as orally administered) during passage through the gastrointestinal tract with variable pH (1−7.4). Bioavailability is a very important parameter as it dictates the solid dosage form based on the extent of the metabolism of a drug. ALO in a commercial

https://doi.org/10.1021/acsomega.3c05263
ACS Omega 2023, 8, 34120−34133

tablet dosage form (Zyloprim 300 mg) exhibits an absolute bioavailability of 67 ± 23% with a maximum peak plasma concentration (C_{max}) within an hour.[40,52] It is anticipated that the enhanced dissolution/diffusion profile of ALO salts may improve the pharmacokinetic profile of the native drug. The pharmacokinetics of ALO and its salt hydrates was examined on healthy BALB/c mice following oral administration of 30 mg/kg dose, and bioavailability was accessed by measuring the C_{max} and AUC using UPLC-MS/MS. The pharmacokinetic parameters of ALO and its salts are summarized in Table 2.

Table 2. Mean Pharmacokinetic Parameters of ALO and Its Salts in Mice Plasma

test compound	dose (mg/kg)	$T_{1/2}$ (h)	T_{max} (h)	C_{max} (ng/mL)	AUC_{0-24h} (ng/mL·h)
ALO	30	1.70	0.5	7011 ± 187	36,867 ± 3680
ALO−OXA (hydrate)	30	1.60	0.5	10,483 ± 234 (×1.5)	42,670 ± 4688 (×1.2)
ALO−MLE (hydrate)	30	1.71	0.5	15,984 ± 3 (×2.3)	69,645 ± 7538 (×1.9)

The results showed that there was no detectable drug after 6 h of administered dose due to the fast metabolism to its active metabolite oxypurinol.[40] As expected, ALO salts achieved higher (1.5−2.3-fold) C_{max} within half an hour compared to the native drug (refer Figure 9). Surprisingly, there was no improvement in the half-life of the native drug ALO as both the salts exhibited a similar time period.

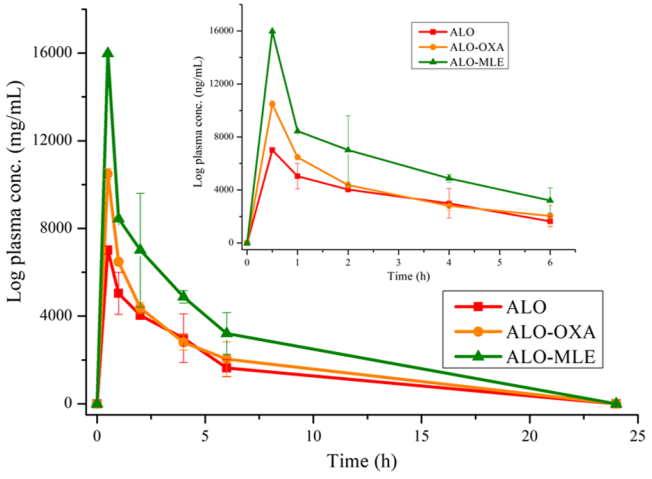

Figure 9. Plasma concentration vs time profile of the ALO and its salt hydrates in mice. Refer the inset for a more clear representation of the plot.

Since ALO and its active metabolite oxypurinol are primarily eliminated only by the kidney (urinary excretion), accumulation of the drug may result in renal failure.[53] Hence, it is recommended that the dosage of ALO should be reduced in patients with renal impairment. The risk of ALO hypersensitivity syndrome is also increased in patients with acute kidney failure, which is associated with the high dose (200−300 mg) used in the treatment. Higher bioavailability of the ALO−MLE salt hydrate will further help formulation scientists to reduce the highest dose limit and offer a lower solid dosage form (100−150 mg) that will have a positive impact on the patient suffering from chronic kidney disease.

3.8. Moisture and Thermal Stability. The physical/chemical stability of a drug is vital for bulk production and storage during research and development. Generally, salts are highly moisture sensitive and get easily deliquescent under high humidity conditions.[9] Even salts are more likely to disintegrate or degrade when exposed in the moist environment for a long time. At ambient conditions (25−35 °C, 60−80% RH), the synthesized ALO salts were stored in a glass vial and found to be stable for more than 6 months. Further, the salts maintained its unique phase when exposed to 30 ± 5 °C, 75 ± 5% RH even after 4 weeks, which was confirmed by PXRD data (refer Figure S9, SI). These salts are exceptionally stable, and there was no change of solid phases after 8 weeks of humidity exposure. To examine the thermal stability of the ALO salts, the corresponding powder forms were kept at 110 °C for an hour in an oven that indicates that ALO−OXA salt hydrate retained as it was, whereas ALO−MLE salt hydrate partially transformed to the native drug (refer Figure S10, SI). The phase transformation of ALO−MLE salt hydrate can be explained based on its dehydration temperature at 107−110 °C. However, ALO−MLE salt (hydrate) is stable at 60 °C when exposed to heat for an hour. This suggests that nonstoichiometric hydrate (e.g., ALO−OXA) may not be always unstable and reluctant to escape from its host structure. To summarize, ALO salt hydrates are exceptionally stable under humid and thermal conditions.

4. CONCLUSIONS

ALO, a structural analogue of purine base hypoxanthine, exhibits poor absorption due to low solubility/permeability and rapid metabolization to oxypurinol. Since it is an ionizable basic drug, salts were prepared with maleic acid and oxalic acid to improve its dissolution, diffusion, and pharmacokinetics. The ionization of the ALO salt hydrates was confirmed by FT-IR data and additionally characterized by DSC/TGA. As ALO salt hydrates quickly disintegrate during crystallization, their crystal structures were solved using Rietveld refinement from high-resolution PXRD data. Among the salts, ALO−MLE maintains stoichiometric hydrate, whereas ALO−OXA manages nonstoichiometric hydrate. ALO−MLE salt hydrate maintains zigzag patterns, whereas ALO−OXA salt hydrate exhibits a planar structure similar to the native drug. Both the salts improved dissolution/solubility by 3−5-fold and diffusion/permeability up to 12-fold when compared to the native drug in a pH 6.8 phosphate buffer medium. Improved dissolution and diffusion aspects of ALO−MLE salt hydrate further increased the peak plasma concentration of the drug in mice during pharmacokinetic evaluation that will enhance absorption in the intestinal membrane. In addition, the salt hydrates were exceptionally stable under high humid and temperature conditions that favor long-term storage. To conclude, ALO−MLE salt hydrate, a promising solid dosage form with improved drug properties, makes it feasible to commercialize the product with ease in industrial production and storage.

■ ASSOCIATED CONTENT

Supporting Information

The Supporting Information is available free of charge at https://pubs.acs.org/doi/10.1021/acsomega.3c05263.

https://doi.org/10.1021/acsomega.3c05263
ACS Omega 2023, 8, 34120−34133

Hydrogen-bond geometry, summary of cocrystal screening, Rietveld plots, H-bonding aspects, XRD pattern comparison, ^{1}H NMR spectra, and SEM images (PDF)
Crystallographic data for ALO−MLE (CIF)
Crystallographic data for ALO−OXA (CIF)

AUTHOR INFORMATION

Corresponding Authors

Vladimir V. Chernyshev − *Department of Chemistry, M. V. Lomonosov Moscow State University, Moscow 119991, Russian Federation; A. N. Frumkin Institute of Physical Chemistry and Electrochemistry RAS, Moscow 119071, Russian Federation;* orcid.org/0000-0001-8514-7471; Email: vladimir@struct.chem.msu.ru

Palash Sanphui − *Department of Chemistry, Faculty of Engineering and Technology, SRM Institute of Science and Technology, Chennai, Tamil Nadu 603203, India;* orcid.org/0000-0001-7854-1964; Email: palashi@srmist.edu.in

Authors

Richu Bagya Varsa S − *Department of Chemistry, Faculty of Engineering and Technology, SRM Institute of Science and Technology, Chennai, Tamil Nadu 603203, India*

Noopur Pandey − *Solid State Pharmaceutics Research Laboratory, Department of Pharmaceutical Sciences & Technology, Birla Institute of Technology, Ranchi 835215 Jharkhand, India;* orcid.org/0000-0003-4014-3615

Animesh Ghosh − *Solid State Pharmaceutics Research Laboratory, Department of Pharmaceutical Sciences & Technology, Birla Institute of Technology, Ranchi 835215 Jharkhand, India;* orcid.org/0000-0002-2990-4738

Anubha Srivastava − *Department of Physics, University of Lucknow, Lucknow 226007 Uttar Pradesh, India*

Pavan Kumar Puram − *Foundation for Neglected Disease Research, Doddaballapur, Bangalore 561203, India*

Sai Teja Meka − *Foundation for Neglected Disease Research, Doddaballapur, Bangalore 561203, India;* orcid.org/0009-0009-8190-3722

Complete contact information is available at: https://pubs.acs.org/10.1021/acsomega.3c05263

Author Contributions

The manuscript was written through contributions of all authors. All authors have given approval to the final version of the manuscript.

Notes

The authors declare no competing financial interest.

ACKNOWLEDGMENTS

P.S. and R.B.V.S. acknowledge the Department of Science and Technology (DST) for improvement of S & T Infrastructure (FIST) with grant no. SR/FST/CST-266/2015(c) for the funding support. A.S. acknowledges the financial support provided by DST with award no. WOS-A/CS-110/2021 toward this research work.

REFERENCES

(1) Liewer, S.; Huddleston, A. N. Oral targeted therapies: managing drug interactions, enhancing adherence and optimizing medication safety in lymphoma patients. *Expert Rev. Anticancer Ther.* **2015**, *15*, 453−464.

(2) Berry, D. J.; Steed, J. W. Pharmaceutical Cocrystals, Salts and Multicomponent Systems: Intermolecular Interactions and Property Based Design. *Adv. Drug Delivery Rev.* **2017**, *117*, 3−24.

(3) Bhalani, D. V.; Nutan, B.; Kumar, A.; Chandel, A. K. S. Bioavailability Enhancement Techniques for Poorly Aqueous Soluble Drugs and Therapeutics. *Biomedicines* **2022**, *10*, 2055.

(4) Kapczynski, A.; Park, C.; Sampat, B. Polymorphs and Prodrugs and Salts (Oh My!): An Empirical Analysis of "Secondary" Pharmaceutical Patents. *PLoS One* **2012**, *7*, No. e49470.

(5) Ji, X.; Wu, D.; Li, C.; Li, J.; Sun, Q.; Chang, D.; Yin, Q.; Zhou, L.; Xie, C.; Gong, J.; Chen, W. Enhanced Solubility, Dissolution, and Permeability of Abacavir by Salt and Cocrystal Formation. *Cryst. Growth Des.* **2022**, *22*, 428−440.

(6) Mannava, M. K. C.; Gunnam, A.; Lodagekar, A.; Shastri, N. R.; Nangia, A. K.; Solomon, K. A. Enhanced solubility, permeability, and tabletability of nicorandil by salt and cocrystal formation. *CrystEngComm* **2021**, *23*, 227−237.

(7) Palanisamy, V.; Sanphui, P.; Jyothi, V. G. S. S.; Shastri, N. R.; Bolla, G.; Palanisamy, K.; Prakash, M.; Vangala, V. R. *Cryst. Growth Des.* **2021**, *21*, 1548−1561.

(8) Pandey, N.; Ghosh, A. An outlook on permeability escalation through cocrystallization for developing pharmaceuticals with improved biopharmaceutical properties. *J. Drug Delivery. Sci. & Technol.* **2022**, *76*, No. 103757.

(9) Wermuth, C. G.; Stahl, P. H. Eds. *Handbook of Pharmaceutical Salts: Properties, Selection and Use*, Wiley−VCH: Weinheim, Germany, 2002.

(10) Cruz-Cabeza, A. J. Acid−base crystalline complexes and the pKa rule. *CrystEngComm* **2012**, *14*, 6362−6365.

(11) Bolla, G.; Nangia, A. Clofazimine Mesylate: A High Solubility Stable Salt. *Cryst. Growth Des.* **2012**, *12*, 6250−6259.

(12) Allu, S.; Garai, A.; Chernyshev, V. V.; Nangia, A. K. Synthesis of Ternary Cocrystals, Salts, and Hydrates of Acefylline with Enhanced Dissolution and High Permeability. *Cryst. Growth Des.* **2022**, *22*, 4165−4181.

(13) Waterbeemd, H. V. D.; Lennermäs, H.; Artursson, P. *Drug Bioavailability: Estimation of Solubility, Permeability, Absorption and Bioavailability* Wiley-VCH: Weinheim, Germany. 2003.

(14) Dai, X. L.; Li, S.; Chen, J. M.; Lu, T. B. Improving the Membrane Permeability of 5-Fluorouracil via Cocrystallization. *Cryst. Growth Des.* **2016**, *16*, 4430−4438.

(15) Sanphui, P.; Tothadi, S.; Ganguly, S.; Desiraju, G. R. Salt and Cocrystals of Sildenafil with Dicarboxylic Acids: Solubility and Pharmacokinetic Advantage of the Glutarate Salt. *Mol. Pharmaceutics* **2013**, *10*, 4687−4697.

(16) Vener, M. V.; Makhrov, D. E.; Voronin, A. P.; Shalafan, D. R. Molecular Dynamics Simulation of Association Processes in Aqueous Solutions of Maleate Salts of Drug-like Compounds: The Role of Counterion. *Int. J. Mol. Sci.* **2022**, *23*, 6302.

(17) Voronin, A. P.; Surov, A. O.; Churakov, A. V.; Parashchuk, O. D.; Rykounov, A. A.; Vener, M. V. Combined X-ray Crystallographic, IR/Raman Spectroscopic, and Periodic DFT Investigations of New Multicomponent Crystalline Forms of Anthelmintic Drugs: A Case Study of Carbendazim Maleate. *Molecules* **2020**, *25*, 2386.

(18) Pacher, P.; Nivorozhkin, A.; Szabó, C. Therapeutic Effects of Xanthine Oxidase Inhibitors: Renaissance Half a Century after the Discovery of Allopurinol. *Pharmacol. Rev.* **2006**, *58*, 87−114.

(19) *DrugBank online*, For physical properties of allopurinol, refer https://go.drugbank.com/drugs/DB00437.

(20) Prusiner, P.; Sundaralingam, M. Stereochemistry of nucleic acids and their constituents. XXIX. Crystal and Molecular Structure of Allopurinol, a Potent Inhibitor of Xanthine Oxidase. *Acta Crystallogr. Sect. B: Struct. Crystallogr. Cryst. Chem.* **1972**, *B28*, 2148−2152.

(21) Sheldrick, W. S.; Bell, P. Interaction of Metal Ions with Allopurinol Derivatives. Preparation and Structural Characterization of Methylmercury(II) Complexes. *Inorg. Chim. Acta* **1987**, *137*, 181−188.

(22) Ravindra, N. V.; Panpaliaa, G. M.; Sarma, J. A. R. P. Bis[5-oxo-4,5-dihydro-8H-2-azonia-4,8,9-trizabicyclo[4.3.0]nona-2,6,9(1)-tri-

https://doi.org/10.1021/acsomega.3c05263
ACS Omega 2023, 8, 34120−34133

ene] sulfate. *Acta Cryst. Sect. E: Struct. Rep. Online* **2008**, *64*, No. o2411.
(23) Bejagam, S. N.; Fonari, M. S.; Averkiev, B. B.; Khrustalev, V. N.; Lindline, J.; Timofeeva, T. V. Adducts of N-heterocyclic drugs, niacin, allopurinol and amiloride with 2,4-pyridinedicarboxylic acid co-former. *Cryst. Growth Des.* **2017**, *17*, 4237−4245.
(24) Dai, X. L.; Yao, J.; Wu, C.; Deng, J. H.; Mo, Y. H.; Lu, T. B.; Chen, J. M. Solubility and Permeability Improvement of Allopurinol by Cocrystallization. *Cryst. Growth Des.* **2020**, *20*, 5160−5168.
(25) Hussain, A.; Rytting, J. H. Prodrug approach to enhancement of rate of dissolution of allopurinol. *J. Pharm. Sci.* **1974**, *63*, 798−799.
(26) Changdeo, J. S.; Vinod, M.; Shankar, K. B.; Rajaram, C. A. Physicochemical characterization and solubility enhancement studies of allopurinol solid dispersions. *Braz. J. Pharm. Sci.* **2011**, *47*, 513−523.
(27) Radhakrishnan, A.; Palanisamy, V.; Sanphui, P. Organic molecular salts of allopurinol with improved solubility. *Mater. Today: Proc.* **2021**, *40*, S210−S215.
(28) Zhukov, S. G.; Chernyshev, V. V.; Babaev, E. V.; Sonneveld, E. J.; Schenk, H. Application of simulated annealing approach for structure solution of molecular crystals from X-ray laboratory powder data. *Z. Kristallogr. − Cryst. Mater.* **2001**, *216*, 5−9.
(29) Zlokazov, V. B.; Chernyshev, V. V. MRIA - a program for a full profile analysis of powder multiphase neutron-diffraction time-of-flight (direct and Fourier) spectra. *J. Appl. Crystallogr.* **1992**, *25*, 447−451.
(30) Richu Bagya Varsa, S.; Sanphui, P.; Chernyshev, V. Polymorphs and isostructural cocrystals of dexamethasone: towards the improvement of aqueous solubility. *CrystEngComm* **2022**, *24*, 6045−6058.
(31) Popa, N. C. The (hkl) Dependence of Diffraction-Line Broadening Caused by Strain and Size for all Laue Groups in Rietveld Refinement. *J. Appl. Crystallogr.* **1998**, *31*, 176−180.
(32) Ahtee, M.; Nurmela, M.; Suortti, P.; Järvinen, M. Correction for preferred orientation in Rietveld refinement. *J. Appl. Crystallogr.* **1989**, *22*, 261−268.
(33) Järvinen, M. Application of symmetrized harmonics expansion to correction of the preferred orientation effect. *J. Appl. Crystallogr.* **1993**, *26*, 525−531.
(34) Makkar, P.; Ghosh, N. N. A review on the use of DFT for the prediction of the properties of nanomaterials. *RSC Adv.* **2021**, *11*, 27897−27924.
(35) Frisch, M. J.; Trucks, G. W.; Schlegel, H. B.; Scuseria, G. E.; Cheeseman, J. R.; Robb, M. A.; Scalmani, G.; Barone, V.; Mennucci, B.; Petersson, G. A.; Nakatsuji, H.; Caricato, M.; Li, X.; Hratchian, H. P.; Izmzylov, A. F.; Bloino, J.; Zheng, G.; Sonnenberg, J. L.; Hada, M.; Ehara, M.; Toyota, K.; Fukuda, R.; Ishida, J.; Hasegawa, M.; Nakajima, T.; Honda, Y.; Kitao, O.; Nakai, H.; Vreven, T.; Montgomery, Jr., J. A.; Peralta, J. E.; Ogliaro, F.; Bearpark, M.; Heyd, J. J.; Brothers, E.; Kudin, K. N.; Staroverov, V. N.; Kobayashi, R.; Normand, J.; Raghavachari, A.; Rendell, A.; Burant, J. C.; Iyengar, S. S.; Tomasi, J.; Cossi, M.; Rega, N.; Millan, J. M.; Klene, M.; Knox, J. E.; Cross, J. B.; Bakken, V.; Adamo, C.; Jaramillo, J.; Gomperts, R.; Stratmann, R. E.; Yazyev, O.; Austin, A. J.; Cammi, R.; Pomelli, C.; Ochterski, J. W.; Martin, R. L.; Morokuma, K.; Zakrzewski, V. G.; Voth, G. A.; Salvador, P.; Dannerberg, J. J.; Dapprich, S.; Daniels, A. D.; Farkas, J.; Foresman, B.; Ortiz, J. V.; Cioslowski, J.; Fox, D. J. *GAUSSIAN 09*, Revision, Gaussian, Inc.: Wallingford CT, 2009.
(36) Lee, C.; Yang, W.; Parr, R. G. Development of the Colle-Salvetti correlation-energy formula into a functional of the electron density. *Phys. Rev. B* **1988**, *37*, 785−789.
(37) Becke, A. D. Density-functional thermochemistry. IV. A new dynamical correlation functional and implications for exact-exchange mixing. *J. Chem. Phys.* **1996**, *104*, 1040−1046.
(38) Parr, R. G. Density Functional Theory of Atoms and Molecules. *Horizons of Quantum Chemistry*, Springer Dordrecht 1980, Vol. 3, pp. 5−15, ISBN: 978−94−009-9029-6, DOI: 10.1007/978-94-009-9027-2.
(39) Montgomery, J. A., Jr.; Frisch, M. J.; Ochterski, J. W.; Petersson, G. A. A complete basis set model chemistry. VI. Use of density functional geometries and frequencies. *J. Chem. Phys.* **1999**, *110*, 2822−2827.
(40) Iqbal, M.; Ezzeldin, E.; Herqash, R. N.; Alam, O. Ultra-performance hydrophilic interaction liquid chromatography coupled with tandem mass spectrometry for simultaneous determination of allopurinol, oxypurinol and lesinurad in rat plasma: Application to pharmacokinetic study in rats. *PLoS One* **2019**, *14*, No. e0213786.
(41) Groom, C. R.; Bruno, I. J.; Lightfoot, M. P.; Ward, S. C. The Cambridge Structural Database. *Acta Crystallogr. Sect. B: Struct. Sci. Cryst. Eng. Mater.* **2016**, *72*, 171−179.
(42) Pina, M. F.; Pinto, J. F.; Sousa, J. J.; Fábián, L.; Zhao, M.; Craig, D. Q. M. Identification and Characterization of Stoichiometric and Nonstoichiometric Hydrate Forms of Paroxetine HCl: Reversible Changes in Crystal Dimensions as a Function of Water Absorption. *Mol. Pharmaceutics* **2012**, *9*, 3515−3525.
(43) Braun, D. E.; Griesser, U. J. Supramolecular Organization of Nonstoichiometric Drug Hydrates: Dapsone. *Front. Chem.* **2018**, *6*, 31.
(44) Saikia, B.; Pathak, D.; Sarma, B. Variable stoichiometry cocrystals: occurrence and significance. *CrystEngComm* **2021**, *23*, 4583−4606.
(45) Jurczak, E.; Mazurek, A. H.; Szeleszczuk, Ł.; Pisklak, D. M.; Zielińska-Pisklak, M. Pharmaceutical Hydrates Analysis—Overview of Methods and Recent Advances. *Pharmaceutics* **2020**, *12*, 959.
(46) Tieger, E.; Kiss, V.; Pokol, G.; Finta, Z.; Dušek, M.; Rohlíček, J.; Skořepová, E.; Brázda, P. Studies on the crystal structure and arrangement of water in sitagliptin L-tartrate hydrates. *CrystEngComm* **2016**, *18*, 3819−3831.
(47) Stephenson, G. A.; Diseroad, B. A. Structural relationship and desolvation behavior of cromolyn, cefazolin and fenoprofen sodium hydrates. *Int. J. Pharm.* **2000**, *198*, 167−177.
(48) Mannava, M. K. C.; Suresh, K.; Nangia, A. Enhanced bioavailability in the oxalate salt of the anti-tuberculosis drug ethionamide. *Cryst. Growth Des.* **2016**, *16*, 1591−1598.
(49) Li, L.; Yin, X. H.; Diao, K. S. Improving the solubility and bioavailability of anti-hepatitis B drug PEC via PEC−fumaric acid cocrystal. *RSC Adv.* **2020**, *10*, 36125−36134.
(50) *Drug Bioavailability: Estimation of Solubility, Permeability, Absorption and Bioavailability* Edited by H., van de Waterbeemd; H., Lennemas; P., Artursson Wiley-VCH: Weinheim, Germany. 2003ISBN 3−527-30438-X, DOI: 10.1021/jm040011t.
(51) Hohenberg, P.; Kohn, W. Inhomogeneous electron gas. *Phys. Rev. B* **1964**, *136*, 864−871.
(52) Helmy, S. A.; El-Bedaiwy, H. M. Pharmacokinetics and Comparative Bioavailability of Allopurinol Formulations in Healthy Subjects. *Clin. Pharmacol. Drug Dev.* **2014**, *3*, 353−357.
(53) Hande, K. R.; Noone, R. M.; Stone, W. J. Severe allopurinol toxicity: description and guidelines for prevention in patients with renal insufficiency. *Am J Med.* **1984**, *76*, 47−56.